Interactive comment on "Rainfall measurement from opportunistic use of earth-space link in Ku Band"

by L. Barthès and C. Mallet

Anonymous Referee #1

Received and published: 22 March 2013

General comments

Comment #1 : The main reason argued for the deployment of such network is the cost but I would argue that the installation costs of such a device may be higher than that of a rain gauge. I see more advantages respect to the maintenance cost since rain gauges require constant surveillance. Therefore I would stress the fact that such setup can provide relatively inexpensive measurements in unpopulated areas where there would be otherwise no measurements at all.

We agree. Some sentences were added/modified in the introduction (See text in blue in the manuscript). A table comparing main features between weather radars, rain gauge networks and Ku device was added.

Comment #2 : I understand the need for a simplified model for the Attenuation-Rain relation but in my opinion the authors should not neglect the temperature dependence. They go a long way analysing the sensitivity to DSD but such relation is much more sensitive to temperature than to DSD.

Specific attenuation depends on temperature through the cross-section. The latter is depending of refractive index of water. But temperature dependence at the considered frequency is not so strong as underlined in section 2.1 :

"*The extinction cross section $\sigma_{fp\theta}(D)$ of raindrops depends on the used frequency, the refractive index n of the water, the size and the shape of the raindrops, the polarization and the incidence angle of the electromagnetic wave. In this study, we consider that $\sigma_{fp\theta}(D)$ is independent of location l even if during the drop fall, the temperature and/or pressure variations can lead to a slight variation of the refractive n. We assume in this study, that the induced variations of $\sigma_{fp\theta}(D)$ are negligible (Atlas, 1977)*".

The figure below shows specific attenuation versus frequency for 3 values of temperature (0, 10, 20°C) and 2 rain rates 10 and 100 mm/h for a Marshall Palmer distribution. In our study the temperature is fixed at 10°C. If we suppose the temperature lies in the range 0 – 20°C, we can see that at 12 GHz when using a temperature of 10C° instead of 0°C or 20°C, the relative error on specific attenuation is about 2% for rain rate equal to 10 mm/h and about 5.5% for rain rates equal to 100 mm/h.

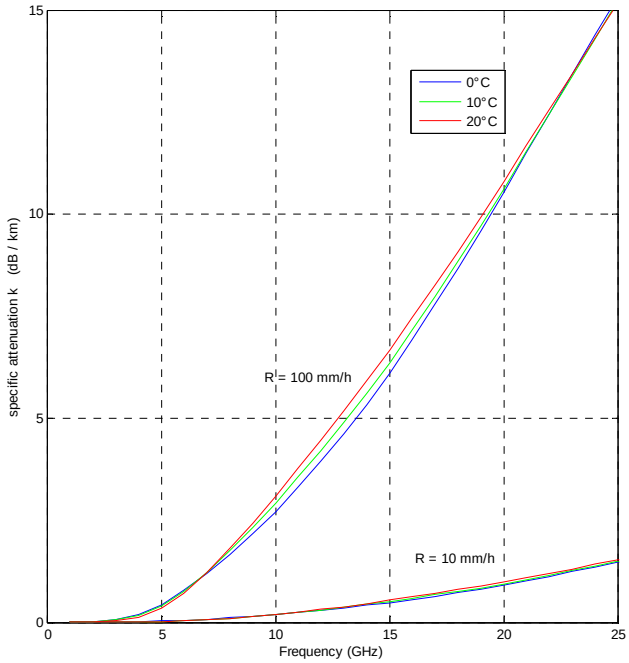

Comment #3 : I do not understand why they use spherical drops to compute R and Kfp from the measured DSDs. There are well established relations between drop size and axis ratios so there is no need for this simplification

Yes we could have used for example Pruppacher and Pitter model to represent ellipsoid raindrops shape and Tmatrix algorithm instead of Mie algorithm to compute specific attenuation. However in the 10-12 GHz band for elevation angles close to 30° the parameters *a* et *b* given by ITU model for horizontal, vertical and circular polarisations of the *k-R* relation are very close to each other (table 2, the 3 last columns). For this reason we used Mie theory which is less computational expensive.

The following sentence is modified to overcome (maybe) an ambiguity:

As we have seen above, k-R relation depends both on the equivalent DSD features that are to say, drops concentration and shape

=> As we have seen above, k-R relation depends both on the equivalent DSD features that are to say, drops concentration and shape of the DSD

Comment #4 : here are many small grammatical mistakes along the text. (I have only pointed some of them in the specific comments). Please consider revision by a native English speaker

Yes the final version will be corrected by a native English speaker. All comments were taken into account. We would like to thank the referee to have accepted to review the paper and to correct the numerous errors of English.

Sincerely

Laurent Barthes, Cécile Mallet

Rainfall measurement from opportunistic use of earth-space link in Ku Band

Laurent Barthès[1], Cécile Mallet[1]

[1] *Université de Versailles Saint-Quentin; CNRS/INSU, LATMOS-IPSL Laboratoire Atmosphères Milieux, Observations Spatiales,.Adresse : Quartier des Garennes, 11 Boulevard d'Alembert, 78280 Guyancourt, France.*

Correspondance to : L. Barthès (laurent.barthes@latmos.ipsl.fr)

Abstract. The present study deals with the development of a low cost microwave device devoted to measure average rain rate observed along earth – satellite links. The principle is to use rain atmospheric attenuation along Earth – space links in Ku band to deduce the path averaged rain rate. These links are characterized by a path length of a few km through the troposphere. Ground based power measurements are carried out by receiving TV channels from different geostationary satellites at Ku-band.

The major difficulty in this study is to retrieve rain characteristics among many fluctuations of the received signal which are due to atmospheric scintillations, changes in the composition of the atmosphere (water vapour concentration, cloud water content) or satellite features (variation of the emitted power, satellite motions). In order to perform a feasibility study of such a device, a measurement campaign has been performed for five months near Paris. This paper proposes an algorithm based on an artificial neural network to identify drought and rainy periods and to suppress the variability of the received signal due to no-rain effects. Taking into account the height of the rain layer, rain attenuation is then inverted to obtain path averaged rain rate. Obtained rainfall rates are compared with co-located rain gauges and radar measurements on the whole experiment period, then the most significant rainy events are analyzed.

1. Introduction

Accurate measurements at medium scale rain intensity and precise localization of precipitation are an important task for the study of the water cycle, and it is also a major element of the physics of climate. Moreover, issues concerning the variability of precipitation in time and space are not only scientific. Knowledge of rainfall variability in the short term (extreme events), and long term (management of water resources), may also help to reduce the human and material damage caused by these phenomena. This study investigates on an inexpensive microwave system to observe rain at medium spatial resolution and at high temporal resolution.

Available sensors for rainfall measurements are principally weather radar, rain gauges, disdrometers and remote sensing satellites. The latter allow global monitoring of precipitation, but the existing microwave sensors have to be placed in low orbit, so as to obtain a resolution of a few kilometres. The corresponding observation frequency is about twice a day which is very low given the dynamics of rainfall events. Moreover, these means of observations are largely confined to the inter tropical region. Ground based weather radar cover areas of about

30,000 km^2, they have revisit in the order of a few minutes and their spatial resolution is about one kilometer. Their financial cost as well as the human means, inevitably associated to them, make their use possible only in particular regions of the earth. Rain gauges allow a punctual observation with a variable time step depending on the intensity of rainfall. Only dense networks of these sensors allow observing the spatial variability of rainy events, moreover the deployment and the maintenance of such networks can be relatively complex and expensive especially in mountainous areas, dense forests, wetlands areas, etc.

Working with operational telecommunication point-to-point microwave links, Upton et al. (2005), Messer et al. (2006), Leijnse et al. (2007), Zinevich et al. (2009), Schleiss et al. (2010), Kaufmann et al. (2011), and Wang et al. (2012) have shown that the path-integrated rain rate can be estimated from attenuation measurements. However ground based microwave link attenuation are provided by telecom operator, which leads to many practical constraints (coarse precision due to quantization error, low temporal resolution (15 min. typically)). Furthermore this kind of data is mainly available in urban areas.

Much of the more than two hundred satellites, deployed by broadcast or telecommunication companies, that orbit the earth, emit a relatively strong microwave signal towards the Earth. They cover almost the entire globe and are located in geostationary orbit. They use microwave frequencies bands, most of them work in Ku band (10.7-12.7 GHz). These satellites, located on a quasi-geostationary orbit, are thus available microwave sources whose position relative to earth is relatively stable. In the band of frequencies used by operators, the transmission is especially affected by the attenuation because of the rain, and some effects less significant but much more frequent due to atmospheric gases (oxygen and water vapor), and non-precipitating water (cloud).

So as to observe rain at an intermediate resolution between radar and rain gauges, we investigate an opportunistic use of these microwave sources to measure rainfall using a low cost and requiring little maintenance device. We have developed a passive, ~~low cost~~ ground based microwave system able to estimate the averaged rain rate along the earth-satellite link (hereafter Ku device). Ground based power measurements are carried out by receiving signals from different geostationary operational satellites in Ku-band like in the experiments carried out by Kumar (2008), Maitra (2007) and Ramachandran (2004). The atmospheric attenuations along earth –space link are then used to deduce the path averaged rain rates. Table 1 summarizes the main characteristics of weather radars, rain gauges network and Ku device.

The paper will investigate how to retrieve the path-average rain rate from received signal obtained in the Ku band. In a first step the measurement principle will be described. The accuracy that can be expected of attenuation measurements in Ku band will be roughly estimated. For this, we used actual time series of raindrop size distribution to estimate attenuation in Ku band and corresponding rain rate in order to study the effect on attenuation of rain inhomogeneity and shape of the raindrop size distribution along the link path. This part gives us a reasonable relationship between atmospheric attenuation and rain rate.

In a second step we describe the experimental device and the measurement campaign we have performed to test the feasibility of rain measurement. Ground based power measurements are carried out by receiving TV channels from different geostationary satellites in Ku-band. The experimental microwave system ~~(hereafter KU device)~~ was installed near Paris during the summer and autumn 2010. The other collocated rain observations (radar, rain gauges) used for comparison are also presented.

The third step deals with methods suggested to retrieve rain rate from the received microwave signal and to quantify the expected rain rate accuracy. In practice, the proposed device only measures a received power and

the difficulty is that the reference level, relative to which the rain attenuation is computed, is not known. In the case of Earth – satellite microwave links, the problem is much more complex than for point-to-point microwave links because the measured level depends on both the atmospheric attenuation through a number of atmospheric processes such as rain, water vapour concentration, cloud water content, turbulence, air temperature, but also to satellite position. The geostationary TV satellites are not really geostationary because most of them have not a circular orbit but a quasi-circular orbit (slightly elliptic) which is not exactly located in the equatorial plane: they have a geosynchronous orbit. This "quasi-geostationary" orbit induces a small relative motion of the satellite (relative to earth) inducing a small change in the direction of the angle of arrival of microwaves and therefore a small change in the received level (depending the antenna aperture).We propose in this section a method to identify drought and rainy periods and to estimate reference level during rainy periods. Finally, taking into account the rain height, estimated rain attenuation is retrieved to obtain path averaged rain rate. The proposed algorithm remains simple because only one channel at a fixed polarization and frequency is used; more sophisticated solutions could be developed in the future by exploiting more channels at different frequencies and polarizations.

In the last section, obtained rain rate are compared with co-located rain gauges and radar measurements. Statistics obtained on the whole experiment period are presented, then the most significant rainy events are analyzed.

2. Physical context

Attenuation is the main propagation effect concerning satellite links operating in the microwave range. This phenomenon is due to several types of atmospheric components: gases, clouds and rain (Ulaby, 1981). Concerning temporal and spatial variability, each of these components have different behaviours. For gas-induced attenuation, the extinction coefficient is equal to the absorption coefficient (Liebe et al. 1993). In the troposphere, the oxygen and the water vapor are the only gases that contribute significantly to absorption in the microwave spectrum. In the case of a satellite slant path, gaseous absorption can be considered to be homogeneous over the horizontal range of a link and variations in gas-induced attenuation are mainly due to variations in water vapor quantity. Gaseous attenuation can’t exceed 0.3 dB at frequencies near 10 GHz and elevation angle of 30° (ITU P.676-9, 2012).

The interaction of electromagnetic wave with tropospheric water particles may involve both absorption and scattering depending their size relatively to the wavelength. Attenuation per unit of volume depends on the density, shape, size distribution, and dielectric properties of the particles contained in the volume. Concerning clouds liquid water, scattering is negligible and the Rayleigh approximation can thus be considered for frequencies up to about 50 GHz (Liebe et al., 1993), the resulting attenuation is proportional to the integrated liquid water content present along the link.. As cloud coverage exhibit important spatiotemporal variability, the corresponding liquid content varies substantially and cloud-induced attenuation can vary strongly but remains below 1 dB for frequencies and elevation angles considered in this study (ITU P840-5, 2012). Concerning ice particles, their absorption coefficient is much smaller than that of water and they do not play a significant role in Ku band. Rain is the major contributor to attenuation in Ku band, both absorption and scattering phenomena play an important role. The attenuation per unit of volume depends on extinction cross section of the water particles and their size distribution profile. This latter varies noticeably both in space and time involving a

specific dynamic of rain-induced attenuation which is different from gases or cloud ones.

2.1. Rain – atmospheric attenuation relationship

Considering scattering effects, the rain specific attenuation $k_{fp\theta}(t,l)$ [dB/km] is related to rain microphysics properties for a given frequency *f*, polarization *p* (*p=H, p=V or p=C* for horizontal, vertical or circular polarization respectively) and an elevation angle θ by the following relation :

$$k_{fp\theta}(t,l) = 4343 \int_{D_{\min}}^{D_{\max}} N(D,t,l)\sigma_{fp\theta}(D)dD \qquad (1)$$

Where $N(D,t,l)$ [m^{-4}] is the rain drop size distribution (DSD), i.e. the number of drops per cubic meter per unit increment of diameter *D*, present in the atmosphere at location *l* and at time *t*, $\sigma_{fp\theta}(D)$ [m^2] is the extinction cross-section for a raindrop of diameter *D* [m].

The rain attenuation $A_{fp\theta}^{Rain}(t)$ [dB] is thus obtained by integrating le specific attenuation along the slant path of length *L*:

$$A_{fp\theta}^{Rain}(t) = \int_0^L k_{fp\theta}(t,l)dl \qquad (2)$$

The extinction cross section $\sigma_{fp\theta}(D)$ of raindrops depends on the used frequency, the refractive index *n* of the water, the size and the shape of the raindrops, the polarization and the incidence angle of the electromagnetic wave. In this study, we consider that $\sigma_{fp\theta}(D)$ is independent of location *l* even if during the drop fall, the temperature and/or pressure variations can lead to a slight variation of the refractive *n*. We assume in this study, that the induced variations of $\sigma_{fp\theta}(D)$ are negligible (Atlas, 1977). Under these conditions, profile of rain along the slant path of length *L* can be considered as a single layer of rain with an equivalent drop size distribution $N_e(D,t)$ [m^{-4}], defined by:

$$N_e(D,t) = \frac{1}{L}\int_0^L N(D,t,l)dl \qquad (3)$$

We can express the equivalent specific attenuation $k_{fp\theta}(t)$:

$$k_{fp\theta}(t) = 4343 \times \int_{D_{\min}}^{D_{\max}} N_e(D,t)\sigma_{fp\theta}(D)dD \qquad (4)$$

Simply related to rain attenuation as follow:

$$A_{fp\theta}^{Rain}(t) = k_{fp\theta}(t) \times L \qquad (5)$$

In practice, the DSD is generally unknown but, considering a gamma drop size distribution the following k-R empirical power law relation between the specific attenuation and rain rate is used instead:

$$k_{fp\theta}(t) = a_{fp\theta} \times R^{b_{fp\theta}}(t) \qquad (6)$$

This expression is shown to be an approximation, except in the low frequency and optical limits (Olsen, 1978). In the field of microwave $a_{fp\theta}$ and $b_{fp\theta}$ depend on frequency and to a lesser extent to the drop size distribution, elevation angle and polarisation.

2.2. Accuracy of the k-R power law relationship

As we have seen above, k-R relation depends both on the equivalent DSD features that are to say, drops concentration and shape of the DSD. These features depend both to atmospheric conditions (convective or stratiform rain for example) and their variability along the radio link *L* (i.e. the considered spatial scale).

We first consider a homogeneous layer with different concentrations and shapes. As pointed out by Jameson (1991) the dependency to the shape for a homogeneous rain layer is related to the frequency. For frequencies close to 25 GHz, the authors show the dependency is weak while larger dispersion appears for lower frequencies especially for f < 9 GHz. In our case the use of 12 GHz links will be expected to be more or less sensitive to rain microphysics. To assess its impact, 1-minute drops size distributions have been computed from rain drops data set collected by a disdrometer (Delahaye et al., 2006) over a period of 24 months between July 2008 and July 2010. By using an approach similar to Leijnse et al. (2010), for each DSD the corresponding rain rate values *R* and specific attenuation values k_{fp} (Eq. 4) were calculated for a frequency of 12 GHz using Mie theory (considering drops shape as spherical). The temperature is taken equal to 10 °C and as rain drops are considered as spherical, obtained specific attenuations are not polarization dependants. Figure 1 shows the obtained scatter plot, the solid line shows the obtained fitted power law and the dashed curve allows comparison with the power law model given by the standard International Telecommunication Union recommendation (ITU-R P.618-9). We can see that the two curves are very similar and are difficult to distinguish from each other. As it can be seen on the figure discrepancy due to microphysics can cause an error of more or less ±7 mm/h for rain rates greater than 10 mm h^{-1}. More precisely, rain rate standard deviation varies from 0.2 to 6 mm h^{-1} for rain rate ranging from 1 to 100 mm h^{-1} leading respectively to relative standard deviations (RSD) between 20% to 6%. This result confirm that the use of a 12 GHz frequency is not optimal for the restitution of low rain rate and thus the proposed device should rather be used for applications for which stronger rain events are relevant (flash flood forecast for example). Table 2 column 2 shows the obtained coefficients by performing the linear regressions on *log(k)-log (R)*. These coefficients are very similar to those given by ITU model (Tab. 2 column 7,8 and 9).

Concerning the variability of the DSD along the radio link, the k-R relations are expected to be sensitive to aggregation over domains of different volumes. Numerous studies, that concern radar measurements, have been devoted to the Z-R power laws relationships between the reflectivity *Z* and the rain rate *R*. Morin et al. (2003) have shown empirically the existence of a scale dependency of Z-R law parameters based on the study of collocated radar and rain gauge data aggregated at different spatial scales. These authors found a quick increase of parameter *a* with scale as well as a moderate decrease of the parameter *b*. Recently Verrier et al. (2012 a, b) quantified the impact of scaling properties of rainfall on Z-R relations using multifractal theory. These authors found that if multifractality behaviour simultaneously holds for *R* and *Z*, the Z-R relationships are characterized by:

$$\begin{cases} b = \text{constant} \\ a \propto l^{K_R(b)} \end{cases} \quad (7)$$

Where $K_R(q)$ defines the "moment scaling function" of rain at order q that entirely characterizes the statistics of the rain field. Usually, $K_R(q)$ is determined by the knowledge of a reduced set of "universal" parameters (Schertzer and Lovejoy, 1987). The coefficient a should therefore be power-law of scale, with scaling exponent that can be demonstrated (from multifractal theory) to be positive when $b>1$ and negative when $b<1$. So as to quantify the impact of scaling properties of rainfall on k-R relations the study performed by Verrier et al. (2012, 2013) relative to the Z-R relationships is applied to the k-R relationships. With a hypothesis of "frozen" atmosphere it can be considered that increasing integration time is equivalent to consider larger spatial scales and thus to obtain k-R relations at different spatial scales. The rain drops dataset previously presented was used again to compute DSD with integration times varying between 1 and 60 minutes and the corresponding k-R relations were computed. Note that the rain rate series have been previously demonstrated to follow multifractal statistics at mesoscale and submesoscale in a detailed study (Verrier et al., 2011). In table 2, the stability of the obtained coefficients associated with the high values of the determination coefficients (R^2 >= 0.972) shows that the k-R relation is quite insensitive to integration time and thus to spatial scale (for the considered frequency). The robustness of the k-R relationship is due to the fact that exponent b is close to 1 (1.17) leading to a less critical to scale dependency of k-R relationships parameters than for the Z-R relationships for which b is close to 1.6. More precisely, in our case $K_R(1.17)$ is equal to 0.03 while $K_R(1.6)$ is equal to 0.12 for reflectivity radar. When considering for example integration times of 1 and 10 minutes, these values lead to a ratio of the prefactor a for *k-R* and *Z-R* relationships respectively equal to 1.07 and 1.31. The latter value show that spatial scale variability can conduct in the case of radar to an important error in some meteorological situations. Concerning the coefficient b, table 2 shows it is almost constant (relative error < 3.5%) as predict by the theory. The stability of the k-R relation deduced from scale properties is relatively well confirmed by empirical values given in Table 2 from 1 to about 30 minutes which correspond to spatial scales between few hundred meters to few km in accordance with the path length L. The k-R estimated parameters are very close to those of the ITU (Recommendation ITU-R P.618-9), for this reason they will be used in the following of the study. Figure 2 shows error statistics between specific attenuations computed from Eq. 4 and those obtained with Eq. 6 and ITU coefficients. A five minutes integration time is selected in order to represent a spatial scale in accordance with Earth – satellite length path L. Obtained bias is comprised between 1 and 6 mm h^{-1} with an absolute relative error less than 10%.

3. Experimental Setup

The experimental system was set up at the LATMOS (Laboratoire Atmosphères, Milieux, Observations Spatiales) in Guyancourt, near Paris, during the summer and autumn 2010. Signals from four geostationary satellites (NSS7, AB1, Thor 5/6, Hotbird 6/8/9) have been received in horizontal polarization, with a multifocus dish antenna of 90 cm diameter. The elevations of link path are close to 30°. For each satellite two 30 MHz width Ku-band channels were received and downconverted by four low-noise block converters (LNBC) to L-

band signals. A RF Switch allows selecting sequentially one of the L-band signals to feed a field analyser. The latter has an accuracy of 0.1 dB and operates in spectrum mode with a 4 MHz bandwidth centered sequentially on the selected channels. The measured level is obtained by averaging five consecutive measurements, then the averaged value is saved by a micro calculator which is used as a data logger. The acquisition sequence records sequentially each of the 8 channels with a sampling period of 2 seconds per channel leading to a total period of 16 seconds (4 satellites × 2 channels x 2 seconds). Fig. 3 shows the experimental set up. The frequencies of each link are given in Table 3. Note that the influence of wet antenna (Leijnse et al., 2008) is not taken into account here, we simply applied a special spray on the LNBs to help removing the droplets. Moreover in the case of Earth-space microwave links only the ground antenna can be wetted.

Independent co-located rain observations are also considered to evaluate the performances of the proposed Ku device: near-by C-band weather radar rain-rate maps provided by Météo France located at Trappes and two rain gauges located at Trappes and Toussus le Noble. The distances between the LATMOS and these places are respectively 2.9 and 3.7 km. Fig. 4 shows the different locations and the directions of the four earth-satellites links (blue lines). The dataset is summarized below:

- 8 time series of received signal $P_{REC}^{ch}(t)$ with ch equal 1 to 8 (4 satellites and 2 channels for each satellite) with a 10 seconds sampling resolution obtained by applying a re-sampling algorithm to the original times series.
- 2 hourly accumulated rainfall time series $R^{RG1}(t)$ and $R^{RG2}(t)$ obtained with the two rain gauges.
- 20 000 radar rain rate maps $R^{rad}(t)$ with a spatial resolution of 1×1 km^2 and temporal resolution of 5 minutes. The relation employed to convert radar reflectivity factors to rain rate is the one used operationally by Météo-France (Tabary, 2007). The period considered covers most of the rainfall events from 23 July to 15 December 2010.

In this first feasibility study, each of the 8 available channels is used independently. Channel 1 is used for the development of algorithms (see section 4), thus seven different values of rain rate are then estimated from other channels. As results obtained with each of the seven remaining channels are quite similar, only those obtained with channel 7 are presented in section 5.

Since microwave links provide path integrated measurements, the corresponding radar path averaged rain rates are calculated from rain maps by averaging the radar pixels $R_i^{rad}(t)$ crossed by the link beam weighted by the corresponding length of the link L_i in the pixel.

For each of the 8 received channels *ch* and each available radar maps $R^{rad}(t)$ the radar average rain rate along the earth-satellite path corresponding to channel *ch* is thus given by : $\overline{R}_{ch}^{rad}(t) = \dfrac{\sum_{i \in I} L_i R_i^{rad}(t)}{\sum_{i \in I} L_i}$

Where $R_i^{rad}(t)$ is the ith pixel (i$\in$ [1, 262144]) of the map, I is the subset of pixels that intersects the path of the satellite corresponding to channel *ch*, and L_i is the length of the link inside the pixel *i*.

Finally, 4 times series $\overline{R}_{ch}^{rad}(t)$ were obtained with a 5 min temporal resolution representing path averaged rain rates on each earth-satellite links according to radar measurements.

Concerning rain gauges we simply averaged the two time series $R^{RG1}(t)$ and $R^{RG2}(t)$ to obtain $\overline{R}^{RG}(t)$. Figure 5 shows the time series $P_{REC}^{ch1}(t), \overline{R}_{ch1}^{rad}(t), \overline{R}_{RG}(t)$ for a 10 days period.

Rainy periods are clearly characterized by a local decrease of the received signal, they thus appear as negative pulses. At the same time, precipitation is also visible on the radar and rain gauges time series. It is also important to note the significant daily variation of the signal (~1 dB) due to satellite motion and antenna aperture as well as a negative trend due to a decrease of temperature and/or water vapour content. For all these reasons, it is very difficult to estimate directly a reference level and thus to deduce the rain attenuation. As explained in the next section, the estimation of the reference level requires first to detect the drought periods from rainy periods taking into account the variability of the signal.

4. Retrieval method

4.1. Reference level

The level of the received signal (P_{REC}) results from the combination of instrumental and geometric characteristics such as power of the transmitter (P_E) on-board the satellite, transmitter and receiver antennas gain G_E, G_R, free space attenuation A_F and tropospheric attenuation (A^{Trop}).

$$P_{REC}(t) = P_E(t) + G_E(t) + G_R(t) - A_F(t) - A^{Trop}(t) \quad \text{(dB)} \tag{8}$$

In practice, P_E and G_E are almost always constants while G_R and A_F vary slowly over time due to satellite motion. Tropospheric attenuation A^{Trop} is critically dependent upon satellite elevation and frequency band. In Ku band as has been stated previously, rain is the dominant contributor to attenuation (A^{Rain}) even if oxygen (A^{Oxygen}), liquid water in clouds (A^{Cloud}), and water vapor (A^{vapor}) and scintillation (A_S) are also present:

$$A^{Trop}(t) = A^{S}(t) + A^{Oxygen}(t) + A^{Cloud}(t) + A^{Vapor}(t) + A^{Rain}(t) \quad \text{(dB)}$$

In order to estimate rain attenuation (A^{Rain}), Eq. 8 is expressed as follows:

$$P_{REC}(t) = P_{REF}(t) - A^{Rain}(t) \quad \text{(dB)} \tag{9}$$

Where $P_{REF}(t)$, called reference level or baseline, is equal to :

$$P_{REF}(t) = P_E + G_E + G_R - A_F - A^{S}(t) - A^{Oxygen}(t) - A^{Cloud}(t) - A^{Vapor}(t) \quad \text{(dB)}$$

In no-rainy situations, we have:

$$P_{REC}(t) = P_{REF}(t) \quad \text{(dB)}$$

The reference level is directly observed during non-rainy situations, it is therefore necessary to estimate it during rain events from reference level obtained during dry periods (Fig. 6). It is thus essentials to dispose of an algorithm allowing differentiating the drought and rainy periods. After the reference level is known, equations 5,

6 and 9 allow estimating the corresponding rain rate $\overline{R}_{ch}^{KU}(t)$.

4.2. The rain – no rain detection algorithm

Each of the atmospheric processes involved has its own dynamics and contributes differently to the wave attenuation. Because of the high heterogeneity of the rain, the latter causes temporal fluctuations faster than gases or clouds of the received signal. To separate drought from rainy periods a similar approach to those used by Kaufmann and Rieckermann (2011) and Schleiss and Berne (2010) was used. Different characteristics (trends, standard deviation, kurtosis, skewness) of the observed Ku band signal received on channel 1 have been computed using different window size from 100 seconds to one hour. Radar data $\overline{R}_{ch1}^{rad}(t)$ have been used to determine the corresponding state of the atmosphere (rainy or dry). The statistical distributions of these characteristics for rainy and dry periods have been compared to test their ability to discriminate between the two states. If it is centered on the time *t* to which the rainfall rate is estimated, the window width *W* should not be chosen too large since it determines the time delay necessary to obtain the estimate. As our goal is to develop, as far as possible, a sensor that allows near real time observation we chose the time windows as small as possible but still guaranteeing good discrimination.

Two characteristics have thus been selected (see Eq. (10)) : the standard deviation over a time window equal to 30 minutes and the local trend over a time window equal to 4 minutes.

$$\begin{cases} std(P_{REC}(n)) = \left[\dfrac{1}{2W+1} \sum_{i=-L}^{L} (P_{REC}(n+i) - \overline{P}_{REC}(n))^2 \right]^{\frac{1}{2}} \text{ with } \overline{P}_{REC}(n) = \dfrac{1}{2W+1} \sum_{i=-L}^{L} P_{REC}(n+i) \text{ and W} = 100 \\ Trd(P_{REC}(n)) = \dfrac{1}{W} \sum_{i=-L}^{L} a_i P_{REC}(n+i) \qquad \text{with a} = (\text{-1,-1,..-1,0,1,..1}) \text{ and } W = 10 \end{cases} \tag{10}$$

Our aim was to obtain a pattern classifier that provides a rule for assigning each sample $P_{REC}(n)$ to one of the two classes (rainy or dry). Because the optimal boundary between the two regions, named decision boundaries, is not linear this provides the principal motivation for using an artificial neural network called Multi –Layer Perceptron (MLP). In fact, the ability of an MLP to learn complex (non-linear) and multi-dimensional mapping from a collection of examples makes it an ideal classifier (Haykin, 1999); The MLP is defined by its topology, namely, the dimensions of the input and output vectors, the number of hidden neurons and by its weights. A training process is necessary to determine the optimal weights. This step is called the training process and requires a representative database composed of a wide set of input and output vectors (X^n, Y^n):

$$\begin{cases} \vec{X}^n = [std(P_{REC}(n)), Trd(P_{REC}(n))] \\ Y^n = \begin{cases} 0 & \text{if } \overline{R}_{ch1}^{rad}(n) < 0.1 \quad \text{belongs to dry period} \\ 1 & \text{if } \overline{R}_{ch1}^{rad}(n) > 0.1 \quad \text{belongs to rainy period} \end{cases} \end{cases} \tag{11}$$

The training data base is composed of half of the data set measured from the channel 1 (1336201 samples), the other half is used to determine the optimal architecture (6 hidden neurons) in terms of generalization ability. The generalization property makes it possible to train an MLP with a representative set of input/target pairs and get good results for predicting unseen input samples. After the training MLP output provides direct estimation of the posterior probabilities (Zhang 2000), Fig. 7.a.

Once obtained MLP can be applied to the entire data set to identify dry and rainy time periods. The discriminating rule is simple: assign sample *n* to rainy class if $Y^n \geq P_o$ or dry class if $Y^n < P_o$. Figure 7.b shows the boundary (solid line) between the two classes. The determination of P_o is detailed hereafter.

After identification of dry and rainy periods from received signal, the reference level is interpolated during rainy periods allowing the estimation of rain attenuation $A^{Rain}(t)$. By using Eq. (12) to express the geometric path length *L* (ITU-R P 618) the specific attenuation $k_{fp\theta}(t)$ is estimated.

$$L = \frac{h_R - h_S}{\sin(\theta)} \qquad (12)$$

where h_R is the rain height given by ITU-R P 530-9 recommendation. The parameter h_S is the altitude of the ground station and θ the elevation angle. Finally, Eq. (6) gives the corresponding rain rate $\overline{R}_{ch1}^{KU}(t)$. The probability threshold P_o (found to be equal to 0.55) is chosen so that the obtained CDF of 1-hour accumulated $\overline{R}_{ch1}^{KU}(t)$ is as close as possible to that of $\overline{R}_{ch1}^{rad}(t)$ (see Fig. 8). One can note that this threshold gives a percentage of rain similar to that obtained with a disdrometer during the same period located at 10 km of the receiver when a threshold of 0.1 mm h^{-1} is applied.

5. Validation and results

The method previously described is used to estimate $\overline{R}_{ch7}^{KU}(t)$. Characteristics vector X, corresponding to channel 7, has been computed from the time series $P_{REC}^{ch7}(t)$ and is applied to the MLP. The threshold P_o allows identifying rainy and dry periods. In order to quantify the performance of the device and associated algorithm, comparison with $\overline{R}_{ch7}^{rad}(t)$ and $\overline{R}^{RG}(t)$ are then performed using different criteria. First, a visual comparison of the obtained times series of rainfall intensities measured by the radar and the Ku device is performed, the order of magnitude and the dynamics of the two measurements are similar (Fig. 9) even if these two quantities cannot be rigorously equal because of the different sampling volumes, altitudes and time resolutions. Fig. 10 shows the comparison of accumulated rainfall measured by the gauges, the radar and those estimated from the received signal for the 4 months period. The radar and the Ku device obtained the same quantity with a total accumulated height of 220 mm while rain gauges measured a slightly higher value.

Fig. 11 shows the comparison of hourly-accumulated rainfall measured by Radar and Ku device (top) and by rain gauge and Ku device (bottom). The quantile – quantile plots (left side) are relatively close to the diagonal indicating that the distributions of 1-hour accumulated rainfall are quite similar. Right plots show error box plot. The medians are close to zero especially between Ku device and radar except for intermediate cumulated rainfall (-1.3 mm). For both box plots, the width of the boxes defined as the width between the 25th and 75th percentiles increases as the cumulated rainfall increases, some explanations are proposed in the next paragraph.

Rain events case studies

Eight rain events of various intensities and durations have been selected. Although we cannot consider they are representative of the local rainfall climatology, they nonetheless allow to highlight a few points. The dates, durations, maximum rain rates and rain amounts estimated by the radar, the pluviometers and Ku device are given in Table 4. Events are sorted by increasing duration. Note that the maximum rain rates R_{max} are obtained with different integration time depending the device (Rain gauges : 1 hour, Radar : 5 mn, Ku device 1 s). It can be seen that rain amount estimated by the radar and the sensor are relatively close to each other (deviation <15%) for events whose duration are between 1 and 3 hours (Events #3,4,5,6). This is not the case for short (< 1 h) nor for long duration events (>6 h). For events of short duration (Events #1,2) the maximum values R_{max} between radar and Ku device are relatively close to each other, but it is difficult to compare the rain amount because of the small size of the rain-cells. Indeed, for small rain-cells crossed more or less perpendicularly by the microwave link, the cell is seen only during a few seconds or minutes while the cell is seen longer in the corresponding pixel radar because its size is much more larger (1 km) than the microwave link (few meters). Thus the two instruments have not necessarily seen the same thing. For long duration rain events (Events #7,8), the reason is completely different, it appears that the basic interpolation method used for the calculation of the reference level is not suitable and a more sophisticated method should be used. It should be noted that in all cases, the comparison between the devices remains difficult for several reasons: (i) it is well known that radar Z-R equation sometimes overestimates or underestimates the rain rate, (ii) path length *L* can be under or overestimated if isotherm zero is not sufficiently well known, (iii) in presence of high rainfall rates which correspond to very strong spatial heterogeneities they can lead to significant differences because the instruments do not see the same volume.

6. Conclusion

Ku band microwave sources on board of satellites such as those employed in telecommunication or broadcasting can potentially be used for the estimation of rainfall. A ground low cost microwave system able to estimate atmospheric attenuation along earth to satellite links has been developed to investigate an opportunistic use of these microwave sources in the band 10.7 – 12.7 GHz. Although this band is not optimal for estimating weak rainfall rates due to its lack of sensitivity, it seems to be a good choice when the rainfall rate increases because the attenuation rarely exceeds 12 dB even in presence of very heavy rains, and it remains easily measurable even with a parabolic antenna of standard size (90 cm).

A 4 months measurement campaign was performed. A Multi-Layer Neural Network was proposed to identify dry and rainy periods from the received signal and thus to estimate the attenuation due to rain on the path link. ITU models were then used to convert rain attenuation into rainfall rate. Good agreement between the Ku device, weather radar and rain gauge in terms of total accumulated rainfall but also in term of hourly rainfall distribution is obtained . Concerning 1-hour cumulated rainfall, discrepancies up to 30% can occur between radar and Ku device. This can be explained by the large difference in sample volume and time integration of the two devices which do not “see” the same thing during heavy rainfall events which are generally associated to very strong spatial heterogeneities. Although the presented results constitute only a partial validation and despite the simplicity of some models and the use of empirical formulas, these first results are promising. It is difficult to compare our results with those obtained by Maitra et al. (2007) who compared rain attenuations with a co-

localized disdrometer and a Simple Attenuation Model (SAM) (Stutzman and Yon, 1986). They conclude that "the discrepancy becomes significant when the rain rates are large (above 30 mm/h) and the corresponding rain cell size is small". The authors explain that for large rain rates, the rain rate decay parameter used in the SAM is not more valid and consequently nothing can be concluded.

Several possibilities could be investigated to improve the performances. In this first feasibility study, each of the available channels (i.e. one frequency and one polarization), is used independently to estimate different values of rain rate. In the future, the combined use of several channels corresponding to different frequencies or polarizations should improve the performances. For long duration rain events (> 3 hours) improvements are still needed, especially in the evaluation of the reference level. Indeed, in this study a simple linear interpolation from dry periods was used. This is only sufficient for short periods in which reference level has little variations. A more sophisticated estimation of the reference level has to be performed for example by representing the reference level with a state-space model associated with a Kalman filter. ITU models were used for the k-R relation and for the estimation of the path length. According to our study the ITU k-R relation perfectly suit our problem, but we do not know about the path length. Other models exist like the one proposed by Adhikari et al. (2011) and should be tested.

The present study deals with the estimation of rainfall rate from a single path link. In the future, the use of several simultaneous links associated with tomography or assimilation methods by using an approach similar to Zinevich et al. (2008, 2009) or Giulli et al. (1997, 1999) could be used to estimate rainfall fields at small-scale and could be helpful in hydrology, flash flood forecasting or for weather radar calibration.

Acknowledgment

This work has been supported by the Programme National de Télédétection Spatiale (PNTS, http://www.insu.cnrs.fr/actions-sur-projets/pnts-programme-national-de-teledetection-spatiale), grant n° PNTS-2013-01. The authors would like to thank M. Parent du Chatelet from Météo France for the various conversations we had on radar data processing.

References

Adhikari, A., Das, S., Bhattacharya, A., and Maitra, A.: Improving rain attenuation estimation: modelling of effective path length using ku-band measurements at a tropical location, Progress In Electromagnetics Research B, Vol. 34, 173-186, 2011.

Atlas, D., and Ulbrich, C. W. : Path- and Area-Integrated Rainfall Measurement by Microwave Attenuation in the 1–3 cm Band. J. Appl. Meteor., 16, 1322–1331, 1977.

Berne, A. and Uijlenhoet, R., : Path-averaged rainfall estimation using microwave links: Uncertainty due to spatial rainfall variability. Geophysical Research Letters, 34 (7), 2007.

Delahaye, J.Y., Barthès, L., Golé, P., Lavergnat, J., Vinson, J.P.: a dual beam spectropluviometer concept, Journal of Hydrology, 328, 110-120, 2006.

Fenicia, F., Pfister, L., Kavetski,D., Matgen, P., Iffly, J.F., Hoffmann, L., Uijlenhoet, R.: Microwave links for rainfall estimation in an urban environment: Insights from an experimental setup in Luxembourg-City. J.of Hydrol., 464–465, 69-78, 2012.

Giuli, D., Facheris, L., and Tanelli, S.: A new microwave tomography approach for rainfall monitoring over

limited areas, Physics and Chemistry of the Earth, 22, 3, 265-273, 1997.

Giuli, D., Facheris, L., and Tanelli, S.: Microwave tomographic inversion technique based on stochastic approach for rainfall fields monitoring, IEEE T. Geoscience and Remote Sensing 37(5), 2536-2555, 1999.

Haykin S. : Neural Networks: comprehensive Foundation, PrenticeHall, Upper Saddle River,N.J, 1999.

ITU-R, Propagation data and prediction methods required for the design of terrestrial line-of-sight systems: Recommendation ITU-R P.530 -9, 2001.

ITU-R, Propagation data and prediction methods required for earthspace telecommunication systems: Recommendation ITU-R P.618-9, ITU-R Recommendations, P-Series Fascicle, ITU, Geneva, 2009.

ITU-R, Attenuation by atmospheric gases, Recommendation ITU-R P.676-9, www.itu.int/rec/R-REC-P.676, 2012.

ITU-R, Specific attenuation model for rain for use in prediction methods : Recommendation ITU-R P.838-3, 2005.

ITU-R, Attenuation due to clouds and fog, Recommendation ITU-R P.840-5, www.itu.int/rec/R-REC-P.840, 2012.

Jameson, A. R.: A Comparison of Microwave Techniques for Measuring Rainfall. J. Appl. Meteor., 30, 32–54, 1991.

Kaufmann, M., Rieckermann, J. : Identification of dry and rainy periods using telecommunication microwave links, 12nd International Conference on Urban Drainage, Porto Alegre/Brazil, 10-15 September, 2011.

Kumar, S., Bhaskara, V., Narayana Rao, D.: Prediction of Ku Band Rain Attenuation Using Experimental Data and Simulations for Hassan, India, Int. J. of Comp. Sci. and Network Security, 8 (4), 2008.

Leijnse, H., Uijlenhoet, R., and Stricker, J.N.M.: Rainfall measurement using radio links from cellular communication networks. Water Resour. Res., 43. 2007.

Leijnse, H., Uijlenhoet, R., Stricker, J.N.M.: Microwave link rainfall estimation: Effects of link length and frequency, temporal sampling, power resolution, and wet antenna attenuation, Advances in Water Resources, 31, 1481–1493, 2008.

Leijnse, H., Uijlenhoet, R., Berne, A.: Errors and Uncertainties in Microwave Link Rainfall Estimation Explored Using Drop Size Measurements and High-Resolution Radar Data. J. Hydrometeor, 11, 1330–1344, 2010.

Liebe, H.J., Hufford, G.A., and Cotton, M.G.: Propagation Modeling of Moist Air and Suspended Water/Ice Particles at Frequencies below 1000 GHz. AGARD Conference, Atmospheric Propagation Effects through Natural and Man-Made Obscurants for Visible to MM-Wave Radiation, 542, 3.1-3.10, 1993.

Maitra, A., Kaustav, C., Sheershendu, B., Srijibendu, B.: Propagation studies at Ku-band over an earth-space path at Kolkata, Indian Journal of Radio Space Physics, 36, 363-368, 2007.

Messer, H., Zinevich, A., and Alpert, P.: Environmental monitoring by wireless communication networks. Science, 312(5774), 713, 2006.

Morin, E., Krajewski, W.F., Goodrich, D., Xiaogang, G., Sorooshian S.: Estimating rainfall intensities from weather radar data: the scale-dependency problem. J. Hydromet., 4, 782-797, 2003.

Olsen, R. L., Rogers, D.V., and Hodge, D.B.: The aRb relation in the calculation of the rain attenuation, IEEE Trans Antennas Propag, 26 (2), 318-329, 1978.

Ramachandran,V., and Kumar, V.: Rain Attenuation Measurement on Ku-band Satellite TV Downlink in Small Island, Electron. Lett., 40(1), 49– 50, 2004.

Schertzer, D., Lovejoy, S.: Physically based rain and cloud modeling by anisotropic, multiplicative turbulent cascades. J. Geophys. Res., 92, 9692-9714, 1987.

Schleiss, M. and Berne, A.: Identification of dry and rainy periods using telecommunciation microwave links. IEEE Geosci. Remote Sens. Lett., 2010.

Stutzman, W. L. and Yon, K. M.: A simple rain attenuation model for earth-space radio links operating at 10–35 GHz, Radio Sci., 21(1), 65–72, 1986, doi:10.1029/RS021i001p00065.

Tabary, P.: The new french operational radar rainfall product. Part I: methodology. Weather Forecast., 22, 393–408, 2007.

Ulaby, F.T., Moore, R.K., Fung, A.K.: Microwave Remote Sensing, Active and Passive, Vol 1, Microwave Remote Sensing Fundamentals and Radiometry, Artech house Inc., 1981.

Upton, G.J.G, Holt, A.R., Cummings, R.J.., Rahimi, A. R. and Goddard, J. W. F., : microwave links: the future for urban rainfall measurement?, Atmos. res., 77, 300-312, 2005.

Verrier, S., Mallet, C., and Barthès, L.: Multiscaling properties of rain in the time domain, taking into account rain support biases. J. Geophys. Res., 116, D20119, doi:10.1029/2011JD015719, 2011.

Verrier, S., Barthes, L., Mallet, C.: Scaling properties of rainfall in space and time and their impact on rain rate estimation from weather radar 7th European Conference on Radar in Meteorology and Hydrology ERAD2012 ,Toulouse France, 2012.

Verrier, S., Barthes L., Mallet C., Theoretical and empirical scale-dependency of Z-R relationships: evidence, impacts and correction, submitted to Journal of Geophysical Research (minor revision), 2013.

Wang, Z., Schleiss, M., Jaffrain, J., Berne, A., Rieckermann, J.: Using Markov switching models to infer dry and rainy periods from telecommunication microwave link signals, Atmos. Meas. Tech., 5, 1847–1859, 2012.

Zhang, G.P.: Neural Networks for Classification: A Survey, IEEE Trans. Syst., Man, Cybern., Part C: applications and reviews, vol. 30, No. 4, 451-462, 2000.

Zinevich, A., Messer, H., Alpert, P.: Frontal Rainfall Observation by a Commercial Microwave Communication Network. J. Appl. Meteor. Climatol.,48 ,1317–1334, 2009.

Zinevich, A., Alpert, P., and Messer, H.: Estimation of rainfall fields using commercial microwave communication networks of variable density, A. Water Res., 31, 1470–1480, 2008.

Tables captions

Table 1. Main characteristics of weather radars, rain gauges networks and Ku device

Table 2. Coefficients of linear regression and coefficients of determination obtained by performing the linear regressions on -log (ke) - log(R) scatterplots for a frequency f equal to 12 GHz and integration times varying between 1 and 60 minutes. The three last columns indicate the ITU recommendation coefficients corresponding respectively to horizontal, circular and vertical polarizations at the same frequency

Table 3. Frequency [MHz] of the considered microwave links.

Table 4. Features of the eight selected events

Figures captions

Fig. 1. Scatter plot of rain rate versus specific attenuation computed from drop size distribution and Mie theory for a frequency f equal to 12 GHz and a time resolution of 1 min. The continuous line indicates the corresponding fitted k-R power law. The dotted line indicates the ITU power law for horizontal polarization.

Fig. 2. Error induced on rain estimation when the ITU power law is used for an integration time equal to 5 min. For each rain bin, the box-and-whiskers diagram indicates the median (the central vertical line), and the lower and upper quartiles (left and right edges of the box). The whiskers indicate the lower and upper limits of the distribution within 1.5 times the interquartile range from the lower and upper quartiles, respectively.

Fig. 3. Experimental setup.

Fig. 4. Locations of the different sites and satellites path links.

Fig. 5. Example of obtained time series: received signal (blue curve), radar rain rate (red curve), 1-hour accumulated rainfall time series (dash green curve).

Fig. 6. Received signal during a rain event.

Fig. 7. a. MLP output : posterior probability of rainy class. **b.** Boundary of the classifier (green solid line), samples corresponding to dry class are in blue, samples corresponding to rainy class are in red.

Fig. 8. Percentage of rain vs 1-hour accumulated rain threshold for the radar time series (green), pluviometers (red), KU device (blue) for a threshold $P_o = 0.55$.

Fig. 9. Example of time series obtained by Ku device (red curve) and Radar (blue curve).

Fig. 10. Accumulated rainfall obtained by radar (blue curve), Pluviometer (green curve), attenuation measurements (red curve) during 4 months.

Fig. 11. Q-Q plot between radar and Ku device (top left) and between pluviometers and Ku device (bottom left). Box plot between radar and Ku device (top right) and between pluviometers and Ku device (bottom right).

Tables

Table 1.

	Typical temporal Resolution	Typical spatial Resolution	Area	Cost (purchase and installation)	Maintenance
Radar	5 min	1 km^2	30000 km^2	****	***
Rain gauge network	1 min – 24h	Ponctual	Proportional #pluviometers	**	***
KU device using one satellite	10 s	5-6 km	5-6 km	*	*
KU device using all available satellites	10 s	~1 km^2	~20 km^2	*	*

Table 2

	1 min	5 min	10 min	30 min	60 min	ITU (H)	ITU (C)	ITU (V)
A	0.027	0.028	0.030	0.030	0.033	0.024	0.024	0.024
B	1.15	1.14	1.13	1.12	1.1	1.17	1.15	1.13
R^2	0.987	0.986	0.98	0.992	0.972	na	na	na

Table 3.

Channel	Satellite	Frequency	Channel	Satellite	Frequency
1	NSS7	12604	5	Thor 5/6	12563
2	NSS7	11694	6	Thor 5/6	12688
3	AB1	12722	7	Hotbird 6/8/9	12285
4	AB1	12547	8	Hotbird 6/8/9	12617

Table 4.

Ev #	Date	Duration (h)	R_{max} Rad (mm/h)	R_{max} Pluv (mm/h)	R_{max} Ku (mm/h)	Amount Rad (mm)	Amount Pluv (mm)	Amount Ku (mm)
1	07/23	0.6	25.8	-	22.1	5.8	-	3
2	10/16	0.8	7.3	-	8.3	1.7	-	0.9
3	10/03	1.5	14.4	1.6	20.5	4.9	1.6	5.6
4	08/04	1.65	30.3	0.9	28.4	5.4	1	4.8
5	08/02	1.7	19.7	9.1	40	5.7	9.1	6.7
6	09/07	2.9	7.9	4.3	8.1	8.3	7	7.8
7	08/23	6.0	8.4	3.7	16.6	4.6	5.4	7.6
8	11/08	9.2	12.5	4	7.1	12.2	10.3	5.4

Figures

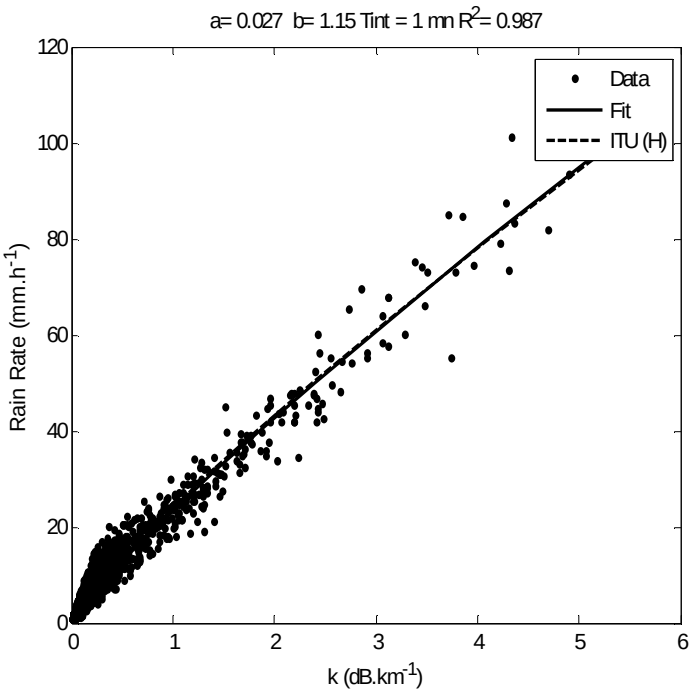

Fig. 1. Scatter plot of rain rate versus specific attenuation computed from drop size distribution and Mie theory for a frequency f equal to 12 GHz and a time resolution of 1 mn. The continuous line indicates the corresponding fitted k-R power law. The dotted line indicates the ITU power law for horizontal polarization.

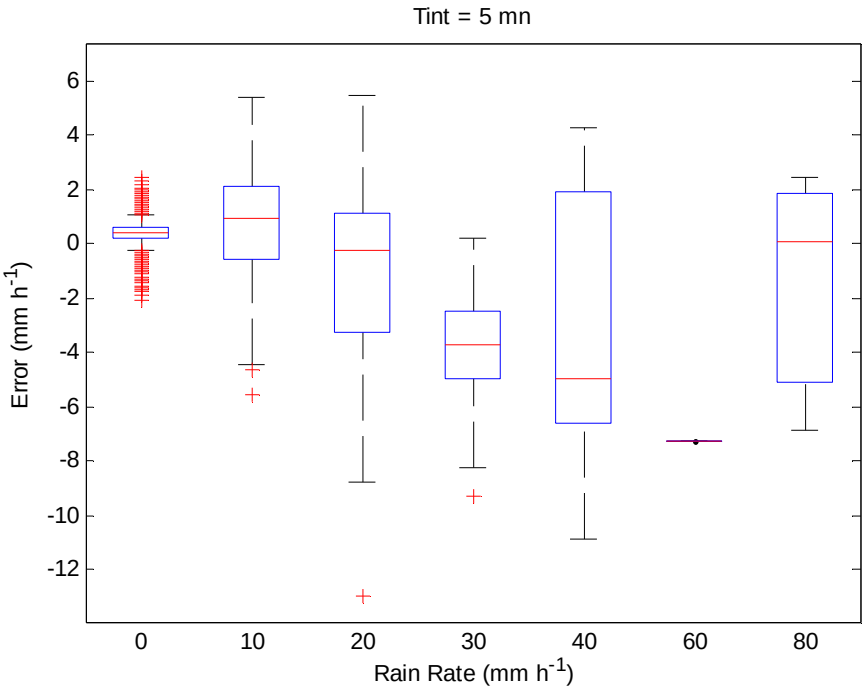

Fig. 2. Error induced on rain estimation when the ITU power law is used for an integration time equal to 5 mn. For each rain bin, the box-and-whiskers diagram indicates the median (the central vertical line), and the lower and upper quartiles (left and right edges of the box). The whiskers indicate the lower and upper limits of the distribution within 1.5 times the interquartile range from the lower and upper quartiles, respectively.

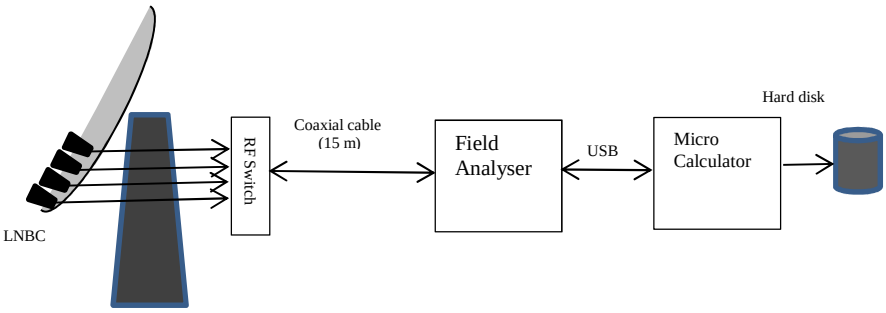

Fig. 3. Experimental setup.

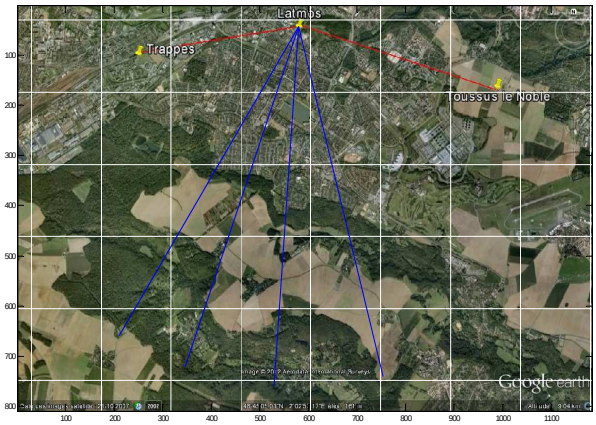

Fig. 4. Locations of the different sites and satellites path links

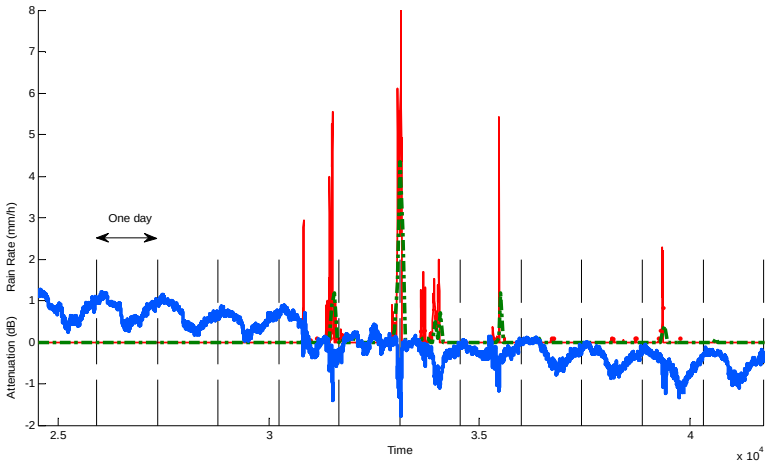

Fig. 5. Example of obtained time series: received signal $P_{REC}^{ch1}(t)$ *(blue curve), radar rain rate* $\overline{R}_{ch1}^{rad}(t)$ *(red curve), 1-hour accumulated rainfall time series* $\overline{R}^{RG}(t)$ *(dash green curve)*

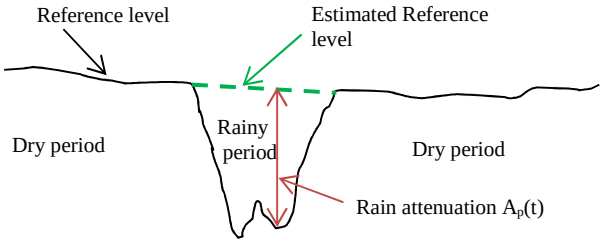

Fig. 6. Received signal during a rain event

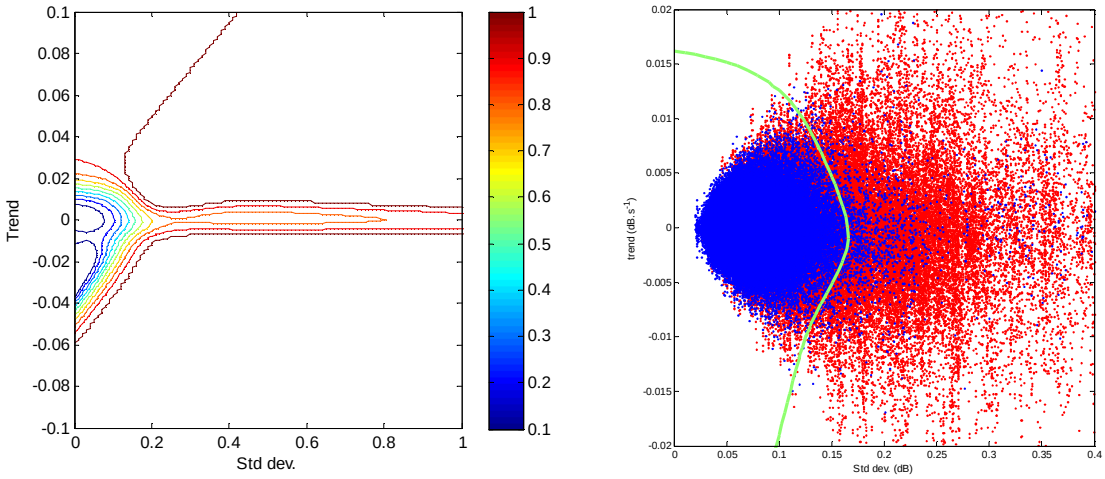

Fig. 7. a. MLP output : posterior probability of rainy class. b. Boundary of the classifier (green solid line), samples corresponding to dry class are in blue, samples corresponding to rainy class are in red.

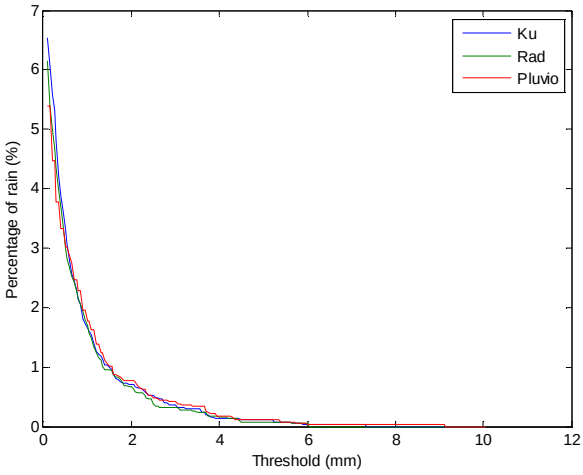

Fig. 8. Percentage of rain vs 1-hour accumulated rain threshold for the radar time series (green), pluviometers (red), KU device (blue) for a threshold P_o = 0.55.

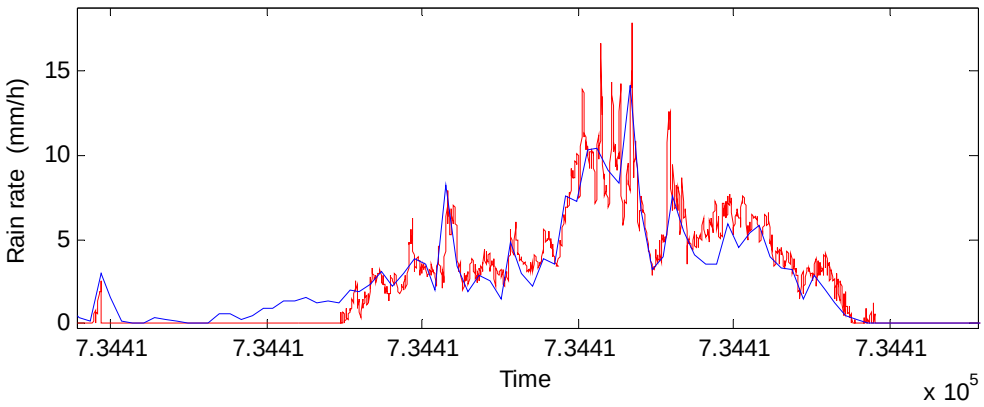

Fig. 9. Example of time series obtained by Ku device (red curve) and Radar (blue curve).

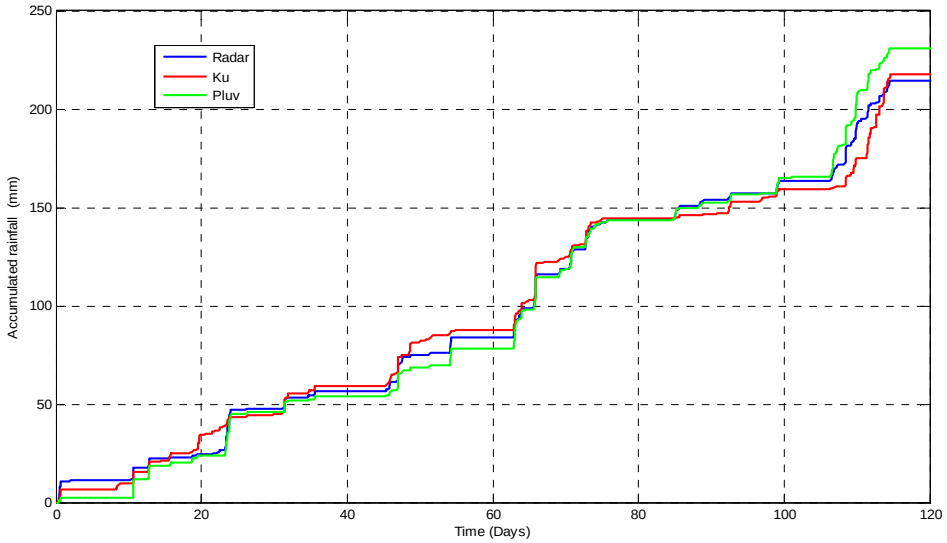

Fig. 10. Accumulated rainfall obtained by radar (blue curve), Pluviometer (green curve), attenuation measurements (red curve) during 4 months.

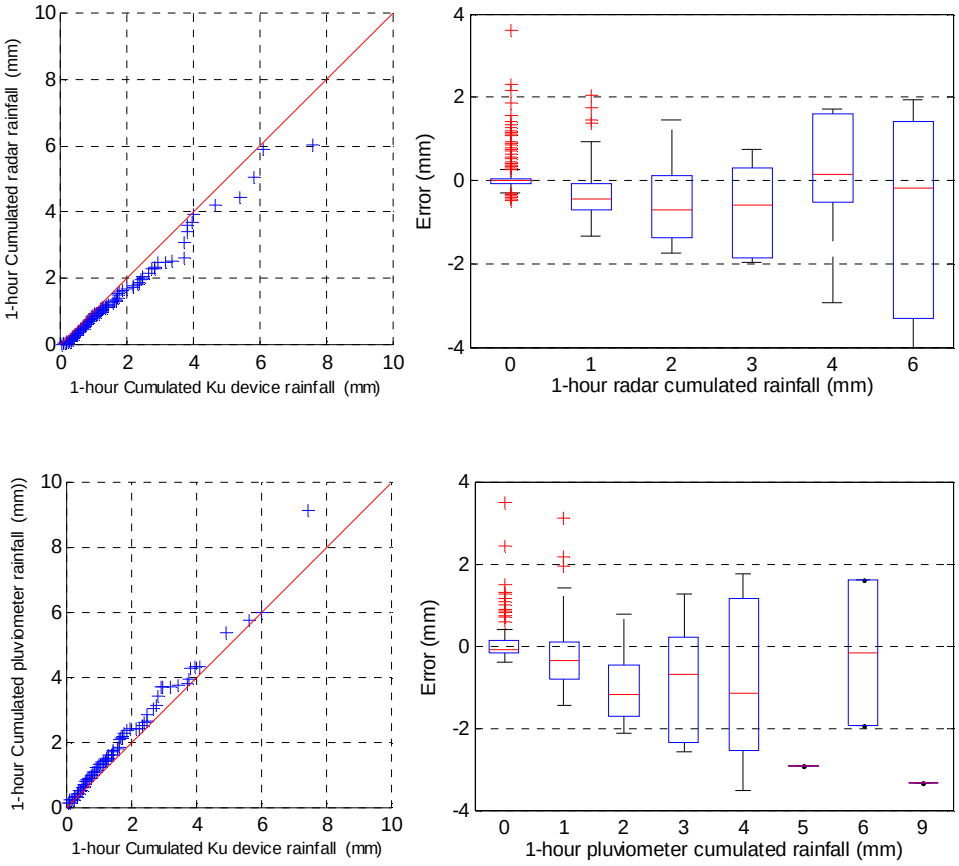

Fig. 11. Q-Q plot between radar and Ku device (top left) and between pluviometers and Ku device (bottom left). Box plot between radar and Ku device (top right) and between pluviometers and Ku device (bottom right).